International Journal of Radiation Oncology biology • physics

www.redjournal.org

Biology Contribution

Effects of Synchrotron X-Ray Micro-beam Irradiation on Normal Mouse Ear Pinnae

Marine Potez, MS,* Audrey Bouchet, PhD,* Jeannine Wagner,* Mattia Donzelli, MS,†,‡ Elke Bräuer-Krisch, PhD,† John W. Hopewell, PhD,§ Jean Laissue, MD,* and Valentin Djonov, MD*

**Institute of Anatomy, University of Bern, Bern, Switzerland; †Biomedical Beamline, European Synchrotron Radiation Facility, Grenoble, France; ‡Joint Department of Physics, The Institute of Cancer Research and the Royal Marsden Hospital, London, United Kingdom; and §Green Templeton College, University of Oxford, Oxford, United Kingdom*

Received Aug 17, 2017, and in revised form Dec 20, 2017. Accepted for publication Feb 5, 2018.

Summary

A high dose of synchrotron micro-beam irradiation with spatial dose distribution did not induce severe damage to superficial tissues in the mouse ear. A transitory reaction of the skin with leukocytic infiltration was seen but only after a peak dose of 800 Gy. Only lymphatic vessels showed long-term alterations after 800 Gy; however, definitive sarcomere damage in striated muscle was seen for peak doses of 200 to 800 Gy. Micro-beam irradiation may

Purpose: To analyze the effects of micro-beam irradiation (MBI) on the normal tissues of the mouse ear.

Methods and Materials: Normal mouse ears are a unique model, which in addition to skin contain striated muscles, cartilage, blood and lymphatic vessels, and few hair follicles. This renders the mouse ear an excellent model for complex tissue studies. The ears of C57BL6 mice were exposed to MBI (50-μm-wide micro-beams, spaced 200 μm between centers) with peak entrance doses of 200, 400, or 800 Gy (at ultra-high dose rates). Tissue samples were examined histopathologically, with conventional light and electron microscopy, at 2, 7, 15, 30, and 240 days after irradiation (dpi). Sham-irradiated animals acted as controls.

Results: Only an entrance dose of 800 Gy caused a significant increase in the thickness of both epidermal and dermal ear compartments seen from 15 to 30 dpi; the number of sebaceous glands was significantly reduced by 30 dpi. The numbers of apoptotic bodies and infiltrating leukocytes peaked between 15 and 30 dpi. Lymphatic vessels were prominently enlarged at 15 up to 240 dpi. Sarcomere lesions in striated muscle were observed after all doses, starting from 2 dpi; scar tissue within individual beam paths remained visible up to 240 dpi. Cartilage and blood vessel changes remained histologically inconspicuous.

Reprint requests to: Valentin Djonov, MD, University of Bern, Institute of Anatomy, Baltzerstrasse 2, 3009 Bern, Switzerland. Tel: (+41) 316318432; E-mail: valentin.djonov@ana.unibe.ch

This work was supported by the Swiss National Foundation and Cancer League.

Conflict of interest: none.

Supplementary material for this article can be found at www.redjournal.org.

Acknowledgments—The authors thank Barbara Krieger for her support in figure preparation. Microscopy was performed on equipment supported by the Microscopy Imaging Center, University of Bern, Switzerland. The authors also thank the Swiss National Science Foundation for the support via the grant n. 31003A_176038 / 1, as well as COST action TD 1205.

https://doi.org/10.1016/j.ijrobp.2018.02.007

be useful for treating skin tumors.

Conclusions: Normal tissues such as skin, cartilage, and blood and lymphatic vessels are highly tolerant to MBI after entrance doses up to 400 Gy. The striated muscles appeared to be the most sensitive to MBI. Those findings should be taken into consideration in future micro-beam radiation therapy treatment schedules.

Introduction

The radiation tolerance of surrounding normal tissues generally limits the radiation dose that can be delivered to the tumor in approximately 60% of all patients treated by radiation therapy (1). Approximately 25 years ago a novel alternative radiation therapy method was developed using synchrotron X rays (2): micro-beam radiation therapy (MRT), based on a spatially and periodically alternating microscopic dose distribution by the spatial distribution of the radiation beam into an array of micro-beams. This allows the deposition of doses of hundreds to thousands of grays in tissue slices in the path of micro-beams (the peak dose) while tissue slices located between micro-beams generally receive only 5% to 10% of the peak dose from scattered radiation (the valley dose) (3, 4). The therapeutic efficiency of MRT has been demonstrated on small laboratory animals bearing different types of tumor (5-12). Normal tissues, which included the brains of adult rats (7, 13-15), the caudal fin of zebrafish (16), immature tissues in suckling rats (17), duck embryos (9), the chick chorioallantoic membrane (18), and piglets (19, 20), have all shown a resistance of normal tissues to micro-beam irradiation (MBI) applied in the MRT mode (21) when compared with conventional uniform field irradiation. The data on MRT effects on normal skin are limited (22, 23), in contrast to those of conventional radiation therapy (24, 25).

In early studies with micro-beams, Zhong et al (22) examined the histologic changes in rat skin of the thigh exposed to very-high-dose MBI (>1000 Gy) and reported a rapid re-epithelialization due to the clonogenic proliferation of cells associated with the hair follicle canal. It has previously been shown (23) that peak MBI dose to the shaved skin on the back of mice caused significantly less damage than uniform radiation exposure using the same dose range.

To examine effects in skin with a lower hair density, resembling, at least in part, human skin, the ears of mice have been irradiated (26, 27). They are composed of a thin epidermis, arranged as 2 to 3 viable layers of keratinocytes, and a thicker dermis, with a low density of elongated fibroblasts. The ear also encloses striated muscle fibers between the dorsal dermis and the cartilage (27). The thin (approximately 200 μm) ear allows a synchronous examination of irradiation-induced reactions of all its tissue components.

The aim of the present study was to analyze temporo-spatial morphologic changes of these tissues after single MBI exposures of 200 Gy, 400 Gy, and 800 Gy at 2, 7, 15, 30, and 240 days after irradiation (dpi).

Methods and Materials

Animals

All the experiments on 8-week-old female C57BL/6J mice were approved by the veterinary office of Bern (Switzerland) under permit BE61/15 and by the European Synchrotron Radiation Facility (ESRF, France) Internal Evaluation Committee for Animal Welfare and Rights (14_ethax22). Mice were anesthetized by an intraperitoneal injection of a mixture of fentanyl 0.05 mg/kg body weight (b.w.), midazolam 5 mg/kg b.w., and medetomidin 0.5 mg/kg b.w. All mice were killed humanely by pentobarbital intraperitoneal injection (50 mg/kg b.w.) before skin sample collection.

Dosimetry

The radiation dose rate, under reference conditions at the beamline ID17 of the ESRF, was measured before the experiment according to the protocol of Fournier et al (28). The resulting dose to the mouse ear was determined by Monte Carlo simulation based on Geant4 (29), which models the ear as a 0.3-mm-thick water disc, 10-mm diameter. The photon spectrum was generated with XOP (30) and is in accordance with the verified spectrum of Crosbie et al (31).

Irradiation

Anesthetized mice were irradiated at the ID17 Biomedical Beamline of the ESRF using synchroton X rays, spatially distributed by a collimator into an approximately 5.5-mm-wide, 14-mm-high array of 27 vertical micro-beams (50-μm width at the half dose maximum [FWHM]), spaced 200 μm apart, center to center (ctc) (32). The mice were placed vertically, head up, the ears maintained by adhesive tape stuck to the outer ear rim to avoid any beam scattering. The array was centered on the dorsal face and covered the entire cranio-caudal aspect of the ear and approximately half of its transversal aspect. Mice were randomly separated in 3 dose groups, exposed to peak entrance doses of 200 Gy, 400 Gy, and 800 Gy. Sham-irradiated animals served as controls at the different time points.

Tissue collection

At 2, 7, 15, 30, and 240 dpi, the mice were perfused under anesthesia with 10 mL of 2% paraformaldehyde and the ears

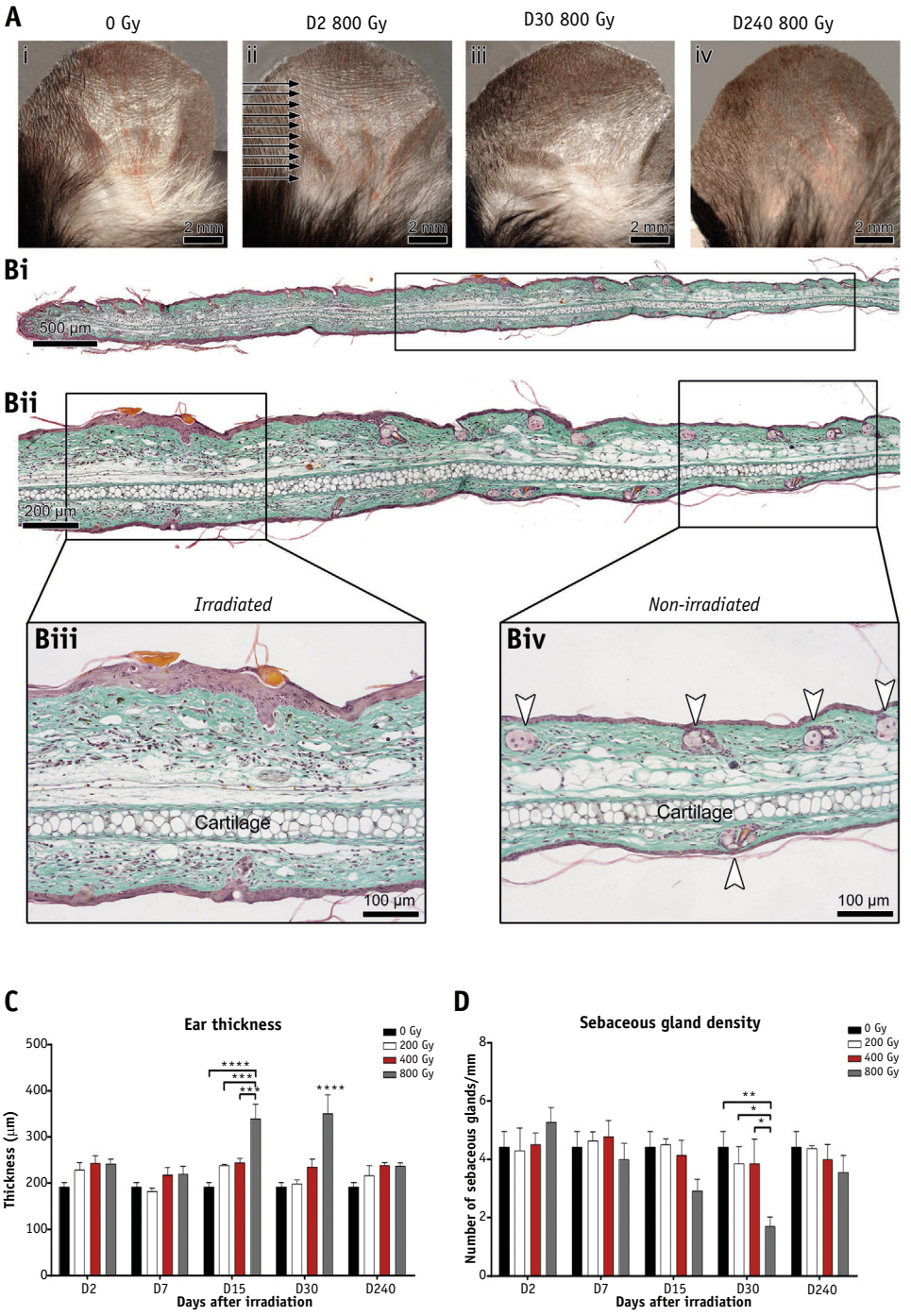

Fig. 1. Macroscopic changes in the mouse ear. (A) (i) Dorsal view of a sham-irradiated "control" ear (identified as 0 Gy in this and other figures) and an ear exposed to 800 Gy at 2 (ii), 30 (iii) and 240 (iv) days after irradiation (dpi). (B) Goldner staining of transverse sections (800 Gy, 15 dpi). (i) Entire ear; (ii) part of "i" containing back to back irradiated (left, iii) and nonirradiated areas (right, iv). Top = dorsal surface. Arrowheads indicate sebaceous glands. (C) Time-related quantitative changes in the full thickness of the ear, as measured in transverse sections. (D) Time-related changes in the number of sebaceous gland (per mm) in the mouse ear. Mean ± standard error of the mean. $*P < .05$, $**P < .01$, $***P < .001$, $****P < .0001$.

processed for conventional light and transmission electron microscopy (TEM) analyses. Four (in irradiated groups) to 6 (in the control group) ears (samples) were collected per dose and per time point.

Histology and immunohistochemistry

Paraffin-embedded tissue sections (5 µm), cut perpendicular to the direction of the micro-beams, were stained with either

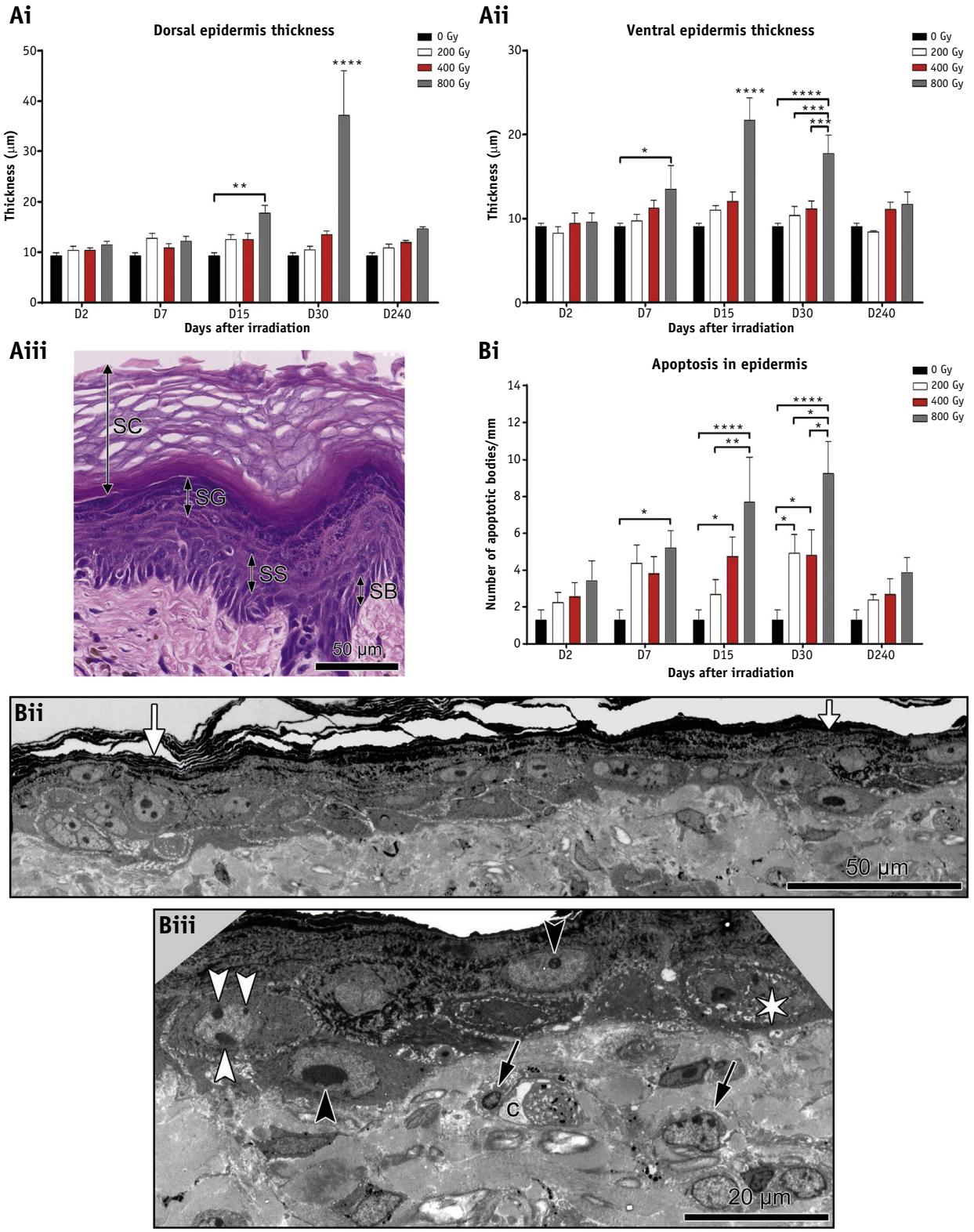

Fig. 2. Epidermal changes in the mouse ear. (A) Time-related changes in the thickness of the dorsal (i) and the ventral (ii) surface of the whole epidermis. (iii) Hyperkeratotic zone in the epidermis at 30 days after irradiation with 800 Gy, with typical epidermal hyperplasia: enlarged stratum corneum (SC), stratum granulosum (SG), stratum spinosum (SS), but normal stratum basale (SB). (B) (i) Time-related changes in the number of apoptotic bodies (per mm) in the epidermis. (ii) Transmission electron microscopy image (15 days after irradiation) of 2 800-Gy peak tracks (white arrows), separated by 150 µm. (iii) Higher-power view of right track. Early apoptosis: chromatin condensation along nuclear membrane (white

hematoxylin and eosin, Goldner, or immunohistochemistry Lyve 1 (ReliaTech, Wolfenbüttel, Germany). Using ImageJ software (https://imagej.nih.gov/ij/), the following parameters were assessed in a 3-mm-long segment of the irradiated field by magnification at ×20 and 5 consecutive areas: the thickness of the epidermal and dermal layers; the number of sebaceous glands per millimeter; the number of lymphatic vessels per millimeter; and lymphatic vessel area (in μm^2/mm). The number of apoptotic bodies was quantified in 2-mm-long segments at magnification ×40, in 6 areas per sample. The leukocyte density was assessed using a semiquantitative arbitrary scoring system (Fig. 3Ci) in the same areas as apoptotic bodies. More details of the staining and measurement are provided in the Supplementary Material and Methods (available online at www.redjournal.org).

Transmission electron microscopy

Samples were fixed in Karnovsky solution followed by osmium tetroxide, washed in sodium cacodylate buffer, dehydrated in graded ethanol, and embedded in EPON (Sigma-Aldrich, Saint-Louis, USA) resin. Blocks were cut with the aid of a Diatome (diamond knife, Biel, Switzerland) diamond knife and stained using uranyl acetate and lead citrate. Sections were examined using a Philips (Philips, Eindhoven, The Netherlands) TEM CM12.

Statistical analysis

Using 2-way analysis of variance with the Tukey posttest program (GraphPad Prism, GraphPad Software, San Diego, CA), values were considered to be significantly different when $P < .05$, and the results are presented as mean ± standard error of the mean.

Results

Macroscopic reaction of the skin after MBI

Micro-beam irradiation exposure, with peak doses of 200 to 800 Gy, did not induce atrophy, necrosis, desquamation, or any other macroscopic alterations in the ear (Fig. 1A). The thickness of the ear after irradiation with 800 Gy was increased at 15 dpi ($P < .001$) and 30 dpi ($P < .0001$), by factors of 1.77 and 1.83, respectively, compared with sham-irradiated ears (Figs. 1B and 1C). No significant effect was observed on sebaceous glands after 200 Gy or 400 Gy (Fig. 1D; $P > .05$), whereas after 800 Gy (30 dpi) the number of sebaceous glands was reduced to 6.0 ± 2.2/mm compared with control values of 15.5 ± 4.6/mm (Figs. 1B and 1D; $P < .01$). No obvious morphologic alterations were observed in the cartilage (Fig. 1B). The stage in the murine hair cycle at the time of irradiation in all ears was compatible with the quiescent telogen stage (33).

Dosimetry

A peak to valley dose ratio of 62 and an output factor (ie, a factor that translates the dose measured under reference dosimetry conditions, using a reference field size, to the dose delivered with the actually applied field size) of 0.971 were calculated for the 5.4-mm-wide field and 15-mm-high micro-beam array traversing the ear. Taking into account an output factor of 0.975 to convert reference dose to peak entrance dose (34), an effective output factor from peak entrance dose to peak dose in the ear of 0.996 applies (ie, a 200-Gy peak entrance dose corresponds to a 199.2-Gy peak dose in the ear, with a valley dose of 3.21 Gy).

MBI effects on the epidermis

The thickness of the dorsal and the ventral epidermis only increased significantly ($P < .05$) after 800 Gy (Fig. 2Ai, ii). At 7 dpi the thickness on the ventral surface was 13.5 ± 5.5 μm ($P < .05$), increasing to 21.7 ± 5.2 μm ($P < .0001$) at 15 dpi compared with sham-irradiated controls (9.1 ± 0.7 μm). The dorsal surface was less effected and was only initially increased on 15 dpi (17.7 ± 3.1 μm vs 9.3 ± 1.3 μm for the sham-irradiated controls; $P < .01$). At 30 dpi the thickness of the ventral and dorsal surface of the epidermis was 37.2 ± 17.7 μm and 17.8 ± 4.2 μm, respectively. This increase in the thickness of the epidermis, after exposure to 800 Gy, related to an overall enlargement of the stratum corneum, stratum granulosum, and stratum spinosum in the entire field of irradiation at 30 dpi. There was moderate enlargement of stratum basale (Fig. 2Aiii).

The number of apoptotic bodies (AB) increased gradually in a dose-dependent manner from 2 dpi forward and became very prominent by 15 dpi and 30 dpi (Fig. 2Bi). The most pronounced effect was observed after 800 Gy. The number of AB increased from 1.3 ± 1.3 AB/mm for the sham-irradiated to 5.2 ± 1.9 AB/mm at 7 dpi and to 9.3 ± 3.5 AB/mm at 30 dpi ($P < .0001$) after 800 Gy. A less dramatic effect was observed after 400 Gy, whereby the number of AB 15 dpi versus 30 dpi remained almost constant (4.8 ± 2 AB/mm [$P < .05$] at 15 dpi to 4.8 ± 2.7 AB/mm [$P < .05$] at 30 dpi). A dose of 200 Gy was associated with a significant increase in the number of AB only at 30 dpi (9.5 ± 4.1 AB/mm; $P < .05$). Transmission electron microscopy revealed qualitative signs of early and late apoptotic changes within in the epidermis and this in

arrowheads), central chromatin condensations, characteristic of autophagy (black arrowhead). Vacuolization of cytoplasm, disrupted nuclear membrane (asterisk): late apoptotic phase. Apoptotic figures in dermal fibroblasts and pericytes (arrows); c = capillary lumen. Mean ± standard error of the mean. *$P < .05$, **$P < .01$, ***$P < .001$, ****$P < .0001$.

the peak tracks at 15 dpi and 30 dpi (Fig. 2Bii, iii). Single fibroblasts and vascular cells occasionally underwent apoptosis within the path of an MB (Fig. 2Biii).

MBI effects on the dermis

After 800 Gy, a significant increase in the thickness of the dorsal surface dermis was seen at 15 to 30 dpi, namely to 178.9 ± 41.3 μm ($P < .0001$) and 153.8 ± 27.6 μm ($P < .05$), respectively, compared with all other irradiated and sham-irradiated groups (Fig. 3Ai). For the ventral surface of the dermis, the thickness after 400 Gy ($P < .05$) and 800 Gy ($P < .001$) was 60.5 ± 10.5 μm and 73.6 ± 12 μm, respectively, at 15 dpi. At 30 dpi, after 800 Gy, the ventral dermal thickness had increased to 92.5 ± 25.3 μm ($P < .0001$) compared with a sham value of 40.7 ± 8.1 μm (Fig. 3Aii). Dermal edema was only observed at 15 dpi and 30 dpi, after 800 Gy (Fig. 3Biii-vi).

After 800 Gy the mean leukocyte density score increased significantly at 7 dpi (0.64 ± 0.24) compared with controls (0.05 ± 0.89; $P < .0001$) and remained significantly higher at 15 dpi (1.27 ± 0.38; $P < .0001$; Fig. 3Civ, vi) and 30 dpi (0.81 ± 0.36; $P < .001$) compared with all the other groups (0.37 ± 0.27 and 0.17 ± 0.11 at 200 Gy, 0.42 ± 0.18 and 0.24 ± 0.22 at 400 Gy at 15 and 30 dpi, respectively; Fig. 3Cii, iii, and v). Transmission electron microscopy studies revealed an infiltration of neutrophils, lymphocytes, and monocytes into the dermis (Fig. 3D).

MBI effects on lymphatics, blood vessels, and peripheral nerves

The number of lymphatic vessels was not significantly modified by MBI compared with sham controls ($P > .05$). However, the total lymph vessel surface per tissue unit area was increased in the 800-Gy group at almost all times after irradiation, to 460.7 ± 173.8 μm^2/mm at 2 dpi, 784 ± 339.6 μm^2/mm at 15 dpi, 723.2 ± 241.5 μm^2/mm at 30 dpi, and 539 ± 333.4 μm^2/mm at 240 dpi compared with controls (137.7 ± 36.3 μm^2/mm; $P < .01$). This increase was significantly higher than that noted in the 200-Gy and the 400-Gy groups at 15 dpi (1.99 times higher after 200 Gy [$P < .01$] and 3.94 times after 400 Gy [$P < .0001$]) and at 30 dpi (9.69 times higher after 200 Gy [$P < .0001$] and 3.02 times after 400 Gy [$P < .001$]). A significant enlargement of lymph vessels was revealed by TEM as early as 2 dpi. Owing to the unchanged number of lymphatic vessels, their endothelium became extremely thin and stained irregularly (Figs. 4D and 4E). The small vessels and peripheral nerves seemed not to be histologically affected even by the highest dose of 800 Gy.

MBI effects on striated muscle cells

Fibers of skeletal muscle cells located above the cartilage in the ear were focally lost after MBI. No obvious differences were found between the different dose levels (Figs. 5A and 5D). The irradiation effects were visible from 2 dpi (Figs. 5A and 5B); sarcomeres were lost and muscle cells vacuolated. Eight months after irradiation, damaged muscled fibers were still visible, surrounded by connective tissue forming a scar (Figs. 5C and 5D).

Discussion

The main corollary from this study is that none of the applied entrance peak doses resulted in any severe early or delayed clinical manifestations of damage, such as moist desquamation, acute ulceration, necrosis, and/or marked atrophy of the auricle. Some clonogenic epidermal cells in the follicular and inter-follicular epidermis must have remained viable and able to repopulate the epidermal cover regions where cells must have died, directly or indirectly, from exposure to the peak entrance doses. This is in keeping with the observation of Priyadarshika et al (23), who did not see full thickness epidermal loss after MRT at entrance doses from 200 Gy to 800 Gy at any time. For an entrance dose of 400 Gy (FWHM ≈ 21-23 μm, 200 μm ctc) they estimated the valley dose to be approximately 4 to 8 Gy, compared with one of 8 to 16 Gy for the entrance dose of 800 Gy (23). These values are in keeping with those in the present study (valley dose of 6.45 Gy and 12.9 Gy for peak entrance doses of 400 Gy and 800 Gy, respectively). Conversely, Zhong et al (22) described a loss of the entire epidermis after MBI peak entrance doses in excess of 1000 Gy (FWHM 90 μm, 300 μm ctc) associated with a valley dose as high as 33 Gy. For conventional broad x-ray beams (290 kVp), the dose required for secondary necrosis in 50% of mouse tails (ED_{50}), by the 7th week after irradiation, is approximately 44 Gy (35). In mice, uniform irradiation of the skin of the back with a 250-kV X ray with a dose of ≈55 Gy (Hopewell, unpublished data) will produce a 100% incidence of moist desquamation within 12 days.

A significant decrease in the number of sebaceous glands was observed 30 dpi after MBI after 800 Gy. Although a slight decrease was seen earlier, at 7 to 15 dpi, they had not all disappeared at these earlier times, in contrast to the observations of Zhong et al (22), who witnessed a total loss after a peak dose of 900 Gy at 6 dpi, which was probably in relation to their higher valley dose.

In the present study only 800 Gy resulted in an increased epidermal and dermal thickness and induced hyperkeratosis on the entrance side of the micro-beam array, most conspicuous at 15 and 30 dpi, as well as a transitory loss of sebaceous glands. Zhong et al (22) also described epidermal hyperplasia, peaking around 2 weeks after MBI at 900 Gy, but this returned to the basal values after

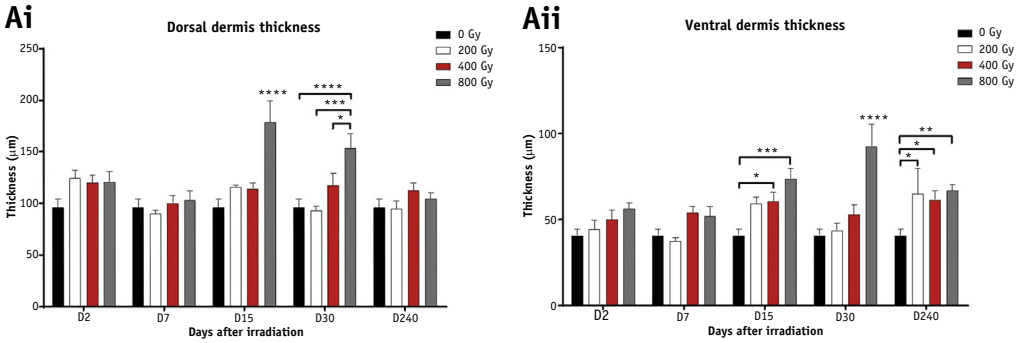

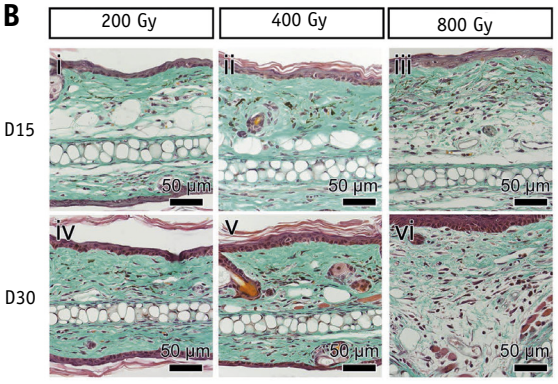

Ci

Parameter	Dermal leukocytic infiltration
Score 0	No leukocytes
Score 1	Leukocytes represent < 10% of the cells
Score 2	Leukocytes represent 10%-25% of the cells
Score 3	Leukocytes represent 25%-50% of the cells
Score 4	Leukocytes represent > 50% of the cells

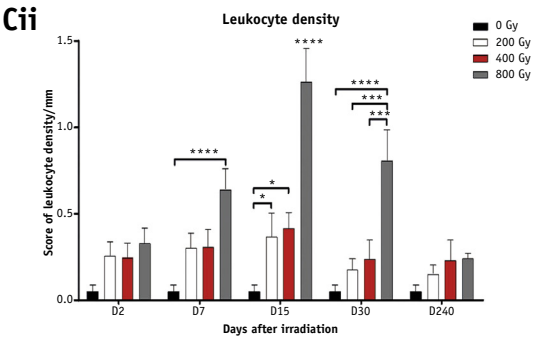

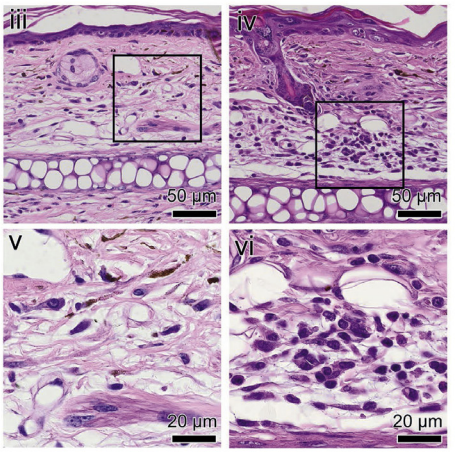

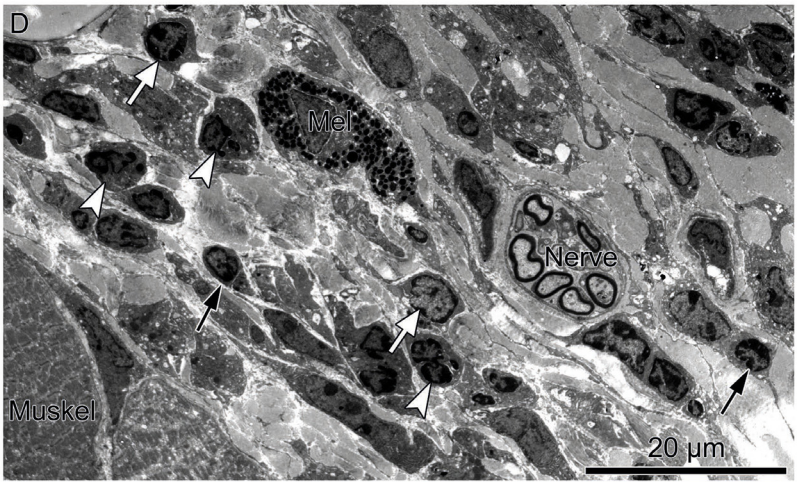

Fig. 3. Dermal changes in the mouse ear. (A) Time-related changes in the thickness of the dorsal (i) and the ventral (ii) dermis in transverse sections. (B) Illustration of tissue increasing edema in transverse histologic sections with dose: 200 Gy (i, iv), 400 Gy (ii, v), 800 Gy (iii, vi) at 15 days after irradiation (dpi) and 30 dpi. Only 800 Gy induced marked edema. (C) Evaluation of the leukocyte infiltration into the dermis (cell count per area). (i) Arbitrary scoring system. (ii) Time-related changes in the leukocyte density score. (iii, v) Low leukocyte density (score 1). (iv, vi) High leukocyte density (score 4). (D) Transmission electron microscopy at 15 dpi showing infiltration of neutrophils (white arrowheads), lymphocytes (black arrows), and monocytes (large white arrows). Mel = melanocyte. Mean ± standard error of the mean. *$P < .05$, **$P < .01$, ***$P < .001$, ****$P < .0001$.

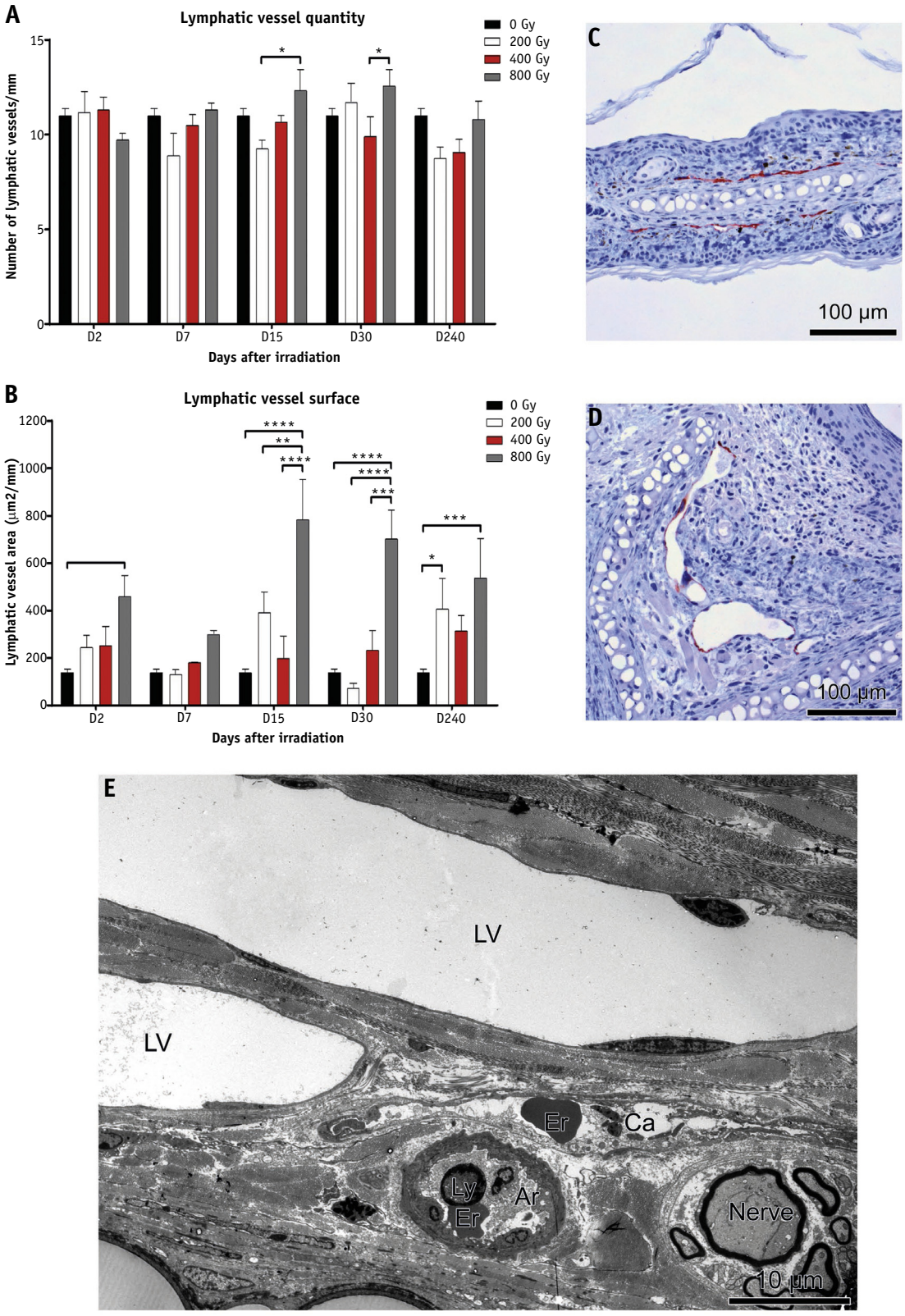

Fig. 4. Lymphatic vessels changes. (A) Time-related changes in the number of lymphatic vessels per mm. (B) Time-related changes in the surface area of lymphatic vessels per mm. (C, D) Immunoreactivity of lymphatic vessels by LYVE-1 Ab (red stain); normal narrow lymphatic vessels on the nonirradiated side (C) and significantly dilated lymphatic vessels 30 days after 800 Gy, irradiated side (D). (E) Transmission electron microscopy showing enlarged lymphatic vessels (LV) with very thin endothelium (800 Gy, 2 days after irradiation). Ar = arteriole; Ca = capillary; Er = erythrocyte; Ly = lymphocyte. Mean ± standard error of the mean. *$P < .05$, **$P < .01$, ***$P < .001$, ****$P < .0001$.

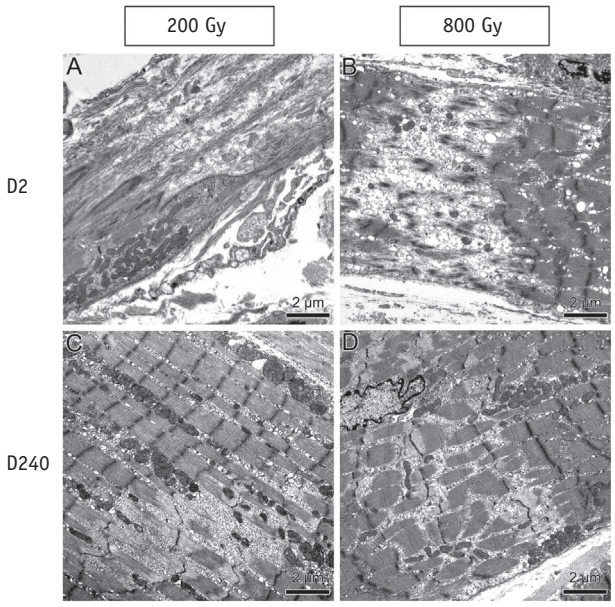

Fig. 5. Changes in striated muscle cells. (A, B) Transmission electron microscopy images of damaged skeletal muscle fibers 2 days after irradiation at 200 Gy and 800 Gy. (C, D) Scar tissue at 240 days after irradiation.

1 month. Those changes were preceded and accompanied by a numerical increase of AB, mainly in the epidermis, mostly in the 800-Gy group, from 7 to 30 dpi. The correlation with the zonal hyperkeratosis began 1 month after exposure to 800 Gy; there were only small, but not uniformly distributed, hyperkeratotic sectors of the epidermis, located within the boundaries of the array but without a detectable micro-beam distribution to the pattern.

Generally the hair follicle cycle in mouse skin lasts over several weeks. Thus, different cycle stages can be present in different animals of the same study, such as the number of epidermal cells located in the hair follicle and hair follicle canal and related to follicular stem cells. Using basic criteria for recognizing key stages of hair follicle growth characterized by schematic drawings and micrographs (27), it was found that the hair follicles of all untreated and irradiated mouse ears in this study were in a quiescent telogenic cycle phase. Therefore, drastic cyclic changes of hair follicle depth and thickness of all skin layers (36) could not have played a role for the interpretation of the present data (33).

Dermal changes included leukocyte infiltration, an increase in the surface areas of lymphatic vessels, and an increased dermal thickness in the 400-Gy and 800-Gy groups (15 and 30 dpi), edema (conspicuous in Fig. 2B, 800 Gy, 30 dpi), and an increase in collagen fibers. The leukocyte infiltration was not confined to the micro-beam paths; neutrophilic granulocytes, lymphocytes, and monocytes were principally localized around blood and lymphatic vessels. Such changes are a well-known consequence of uniform beam irradiation, in which they may be more pronounced than after a corresponding dose delivered by MBI (23).

In this study it is shown for the first time that MBI does not destroy the normal lymphatic vessels in the mouse ear. They appeared normal, with one exception: after 800-Gy (valley dose $\approx$ 12.9 Gy) prolonged dilatation was observed, peaking at 15 and 30 dpi. Comparatively, a uniform beam exposure of the tail of mice to an x-ray dose of 15 or 30 Gy caused significant, dose-dependent increased lymphatic endothelial cell apoptosis and decreased lymphatic function at 28 dpi (37), persisting 84 and 168 dpi, despite resolution of lymphedema in the tail.

Skin erythema after X-irradiation is not generally seen in rodents (38), and no erythematous reaction was observed in the mice in the present study.

For the first time, the effects of MBI on skeletal muscle cells have been observed, confined to the micro-beam paths (peak doses), beginning at 2 dpi. In the valley dose region, the sarcomeres, appearing morphologically intact, maintained the integrity of the muscle tissue architecture. The sites of sarcomere damage remained visible even at 240 dpi, appearing as small scars. It was noted that muscle cells were not totally destroyed because only 50-µm-wide bands of tissue were irradiated with high doses. The most likely reason for the damage is that the ears have been pulled and fixed in the maximal stretched position at the time of irradiation. The created over-extension brings the sarcomeres of striated muscle to such a high tension that even the smallest injury will result in sarcomere disruption. This hypothesis should be investigated in a further study by a comparative study with muscle irradiation in either a contracted or stretched state.

Conclusions

The result of the present experiments showed that the normal tissue had a high tolerance to MBI in the long term. The main effects on the skin induced by MBI at 800 Gy were mostly transitory, whereas only the lymphatic vessels and the muscle cells seemed to remain damaged in the late phase. The minor adverse effects on normal tissues, especially after doses up to 400 Gy, allow the possibility to consider MRT as a promising future strategy for treating superficial tumors without inflicting severe damage to the surrounding normal tissues.

Although still somewhat speculative, the potential clinical value of MRT should perhaps also be discussed in the context of other new innovative approaches to radiation therapy, like the so-called FLASH-radiation therapy, based on ultra-high dose rates (39). Micro-beam radiation therapy (7, 12) and FLASH are both able to increase the differential effect between tumor and normal tissues in experimental animals. Both irradiations can control tumors while inflicting minimal radiation-induced damage to the normal tissues, thereby reducing the risk of adverse side effects. The selective effect may possibly be related to the dose rate. FLASH-radiation therapy is performed using an electron beam produced by an experimental linear acclerator (eRT6) that delivers short pulses ($\leq$500 ms) of radiation at an ultra-high dose rate

(≥40 Gy/s), whereas MRT uses a third-generation synchrotron located at European Synchrotron Radiation Facility, Grenoble, France, with pulses of synchrotron X rays at rates of 15 to 17,000 Gy/s. Moreover, the spatial heterogeneous dose distribution for MRT is a major additional factor compared to the homogeneous irradiation mode in FLASH.

References

1. Orth M, Lauber K, Niyazi M, et al. Current concepts in clinical radiation oncology. *Radiat Environ Biophys* 2014;53:1-29.
2. Slatkin DN, Dilmanian FA, Spanne P. Method for microbeam radiation therapy 1994;1. Patent number US5339347A.
3. Brauer-Krisch E, Serduc R, Siegbahn EA, et al. Effects of pulsed, spatially fractionated, microscopic synchrotron X-ray beams on normal and tumoral brain tissue. *Mutat Res* 2010;704:160-166.
4. Slatkin DN, Spanne P, Dilmanian FA, et al. Microbeam radiation therapy. *Med Phys* 1992;19:1395-1400.
5. Dilmanian FA, Morris GM, Zhong N, et al. Murine EMT-6 carcinoma: High therapeutic efficacy of microbeam radiation therapy. *Radiat Res* 2003;159:632-641.
6. Miura M, Blattmann H, Bräuer-Krisch E, et al. Radiosurgical palliation of aggressive murine SCCVII squamous cell carcinomas using synchrotron-generated X-ray microbeams. *Br J Radiol* 2006;79:71-75.
7. Laissue JA, Geiser G, Spanne PO, et al. Neuropathology of ablation of rat gliosarcomas and contiguous brain tissues using a microplanar beam of synchrotron-wiggler-generated X rays. *Int J Cancer* 1998;78:654-660.
8. Bouchet A, Boumendjel A, Khalil E, et al. Chalcone JAI-51 improves efficacy of synchrotron microbeam radiation therapy of brain tumors. *J Synchrotron Radiat* 2012;19:478-482.
9. Dilmanian FA, Morris GM, Le Duc G, et al. Response of avian embryonic brain to spatially segmented x-ray microbeams. *Cell Mol Biol* 2001;47:485-493.
10. Regnard P, Duc GL, Bräuer-Krisch E, et al. Irradiation of intracerebral 9l gliosarcoma by a single array of microplanar x-ray beams from a synchrotron: Balance between curing and sparing. *Phys Med Biol* 2008;53:861-868.
11. Régnard P, Bräuer-Krisch E, Troprès I, et al. Enhancement of survival of 9L gliosarcoma bearing rats following intracerebral delivery of drugs in combination with microbeam radiation therapy. *Eur J Radiol* 2008;68:S151-S155.
12. Bouchet A, Potez M, Coquery N, et al. Permeability of brain tumor vessels induced by uniform or spatially micro-fractionated synchrotron radiation therapies. *Int J Radiat Oncol Biol Phys* 2017;98:1174-1182.
13. Slatkin DN, Spanne P, Dilmanian FA, et al. Subacute neuropathological effects of microplanar beams of x-rays from a synchrotron wiggler. *Proc Natl Acad Sci U S A* 1995;92:8783-8787.
14. Serduc R, Verant P, Vial JC, et al. In vivo two-photon microscopy study of short-term effects of microbeam irradiation on normal mouse brain microvasculature. *Int J Radiat Oncol Biol Phys* 2006;64:1519-1527.
15. Serduc R, van de Looij Y, Francony G, et al. Characterization and quantification of cerebral edema induced by synchrotron x-ray microbeam radiation therapy. *Phys Med Biol* 2008;53:1153-1166.
16. Brönnimann D, Bouchet A, Schneider C, et al. Synchrotron microbeam irradiation induces neutrophil infiltration, thrombocyte attachment and selective vascular damage in vivo. *Sci Rep* 2016;6:33601.
17. Laissue JA, Lyubimova N, Wagner HP, et al. Microbeam radiation therapy. *Proc SPIE* 1999;3770:38-45.
18. Sabatasso S, Laissue JA, Hlushchuk R, et al. Microbeam radiation-induced tissue damage depends on the stage of vascular maturation. *Int J Radiat Oncol Biol Phys* 2011;80:1522-1532.
19. Laissue JA, Blattmann H, Wagner HP, et al. Prospects for microbeam radiation therapy of brain tumours in children to reduce neurological sequelae. *Dev Med Child Neurol* 2007;49:577-581.
20. Laissue JA, Blattmann H, Di Michiel M, et al. The weaning piglet cerebellum: A surrogate for tolerance to MRT (microbeam radiation therapy) in paediatric neuro-oncology. *Proc SPIE* 2001;4508:65-73.
21. Bouchet A, Serduc R, Laissue JA, et al. Effects of microbeam radiation therapy on normal and tumoral blood vessels. *Phys Med* 2015;31:634-641.
22. Zhong N, Morris GM, Bacarian T, et al. Response of rat skin to high-dose unidirectional microbeams: A histological study. *Radiat Res* 2003;160:133-142.
23. Priyadarshika RCU, Crosbie JC, Kumar B, et al. Biodosimetric quantification of short-term synchrotron microbeam versus broad-beam radiation damage to mouse skin using a dermatopathological scoring system. *Br J Radiol* 2011;84:833-842.
24. Hopewell JW. The skin: Its structure and response to ionizing radiation. *Int J Radiat Biol* 1990;57:751-773.
25. Bolderston A, Lloyd NS, Wong RKS, et al. The prevention and management of acute skin reactions related to radiation therapy: A systematic review and practice guideline. *Support Care Cancer* 2006;14:802-817.
26. Girst S, Greubel C, Reindl J, et al. Proton minibeam radiation therapy reduces side effects in an in vivo mouse ear model. *Int J Radiat Oncol Biol Phys* 2016;95:234-241.
27. Buonanno M, Randers-Pehrson G, Smilenov LB, et al. A mouse ear model for bystander studies induced by microbeam irradiation. *Radiat Res* 2015;184:219-225.
28. Fournier P, Crosbie JC, Cornelius I, et al. Absorbed dose-to-water protocol applied to synchrotron-generated x-rays at very high dose rates. *Phys Med Biol* 2016;61:N349-N361.
29. Allison J, Amako K, Apostolakis J, et al. Recent developments in Geant4. *Nucl Instrum Meth A* 2016;835:186-225.
30. Sánchez del Río M, Dejus RJ. XOP v2.4: Recent developments of the x-ray optics software toolkit. In: Sanchez del Rio M, Chubar O, editors. Advances in Computational Methods for X-Ray Optics II Proceedings Volume 8141. Bellingham, WA: SPIE; 2011. p. 814115.
31. Crosbie JC, Fournier P, Bartzsch S, et al. Energy spectra considerations for synchrotron radiotherapy trials on the ID17 bio-medical beamline at the European Synchrotron Radiation Facility. *J Synchrotron Radiat* 2015;22:1035-1041.
32. Bräuer-Krisch E, Requardt H, Brochard T, et al. New technology enables high precision multislit collimators for microbeam radiation therapy. *Rev Sci Instrum* 2009;80:74301.
33. Müller-Röver S, Handjiski B, van der Veen C, et al. A comprehensive guide for the accurate classification of murine hair follicles in distinct hair cycle stages. *J Invest Dermatol* 2001;117:3-15.
34. Clavel A. Microdosimetrie dans le cadre des essays Precliniques de la radiotheraphie a Microfaisceau [Medical Physics Master thesis]. ESRF, August, 2012.
35. Hendry JH. Radionecrosis of normal tissue: Studies on mouse tails. *Int J Radiat Biol Relat Stud Phys Chem Med* 1978;33:47-55.
36. Hansen LS, Coggle JE, Wells J, et al. The influence of the hair cycle on the thickness of mouse skin. *Anat Rec* 1984;210:569-573.
37. Avraham T, Yan A, Zampell JC, et al. Radiation therapy causes loss of dermal lymphatic vessels and interferes with lymphatic function by TGF-beta1-mediated tissue fibrosis. *Am J Physiol Cell Physiol* 2010;299:C589-C605.
38. Potten CS. The cellular basis of skin injury after cytotoxic insult. *Br J Cancer Suppl* 1986;7:47-58.
39. Favaudon V, Caplier L, Monceau V, et al. Ultrahigh dose-rate FLASH irradiation increases the differential response between normal and tumor tissue in mice. *Sci Transl Med* 2014;6. 245ra93-245ra93.